This article has been accepted for publication in a future issue of this journal, but has not been fully edited. Content may change prior to final publication. Citation information: DOI 10.1109/LAWP.2018.2791660, IEEE Antennas and Wireless Propagation Letters

Ku band low profile asymmetric Bull's-Eye antenna with reduced side lobes and monopole feeding.

U. Beaskoetxea, A. E. Torres-García, M. Beruete

***Abstract*—In this paper, a linearly polarized low profile and asymmetric Bull's-Eye leaky wave antenna fed by a monopole operating at 13 GHz is presented. Broadside radiation from the monopole is achieved by surrounding it with an asymmetric array of semicircular metallic strips on a grounded dielectric slab. With this implementation we demonstrate high gain with a weight of less than 80 g and lower side lobe levels compared to previous designs fed by a resonant slot. The measured antenna shows an experimental gain of 19.4 dBi with only 5 periods and a side lobe level of −16 dB (−20.3 dB for the numerical ideal case at *f* = 12.6 GHz), along with a narrow 6º beamwidth.**

***Index Terms*— Leaky Wave Antenna, Monopole, Asymmetric Bull's-Eye, Grounded Slab**

I. Introduction

AMONG the vast variety of leaky wave antennas (LWA) existing in the literature, there is a certain type that evolves from the enhanced transmission phenomenon [1]–[4], and whose operation principle can be explained following the classic leaky wave theory [5], [6]. These antennas, in their most popular shape, consist of a flat metallic slab pierced by a central slot surrounded by periodic corrugations, either straight and parallel [7], [8] or in the form of a Bull's-Eye (BE) [9]–[12]. Moreover, they are typically fed by a waveguide, and hence have a non-negligible weight that might be detrimental for space or unmanned aerial vehicle applications. Metalized 3D printed structures are a promising path to lighten up the antennas [11], [13]. Another option is to use metasurfaces [14], giving the antenna a competitive lightweight characteristic as well as a very flat profile.

Classical BE antennas employ a symmetric annular periodic structure, a geometry that is optimal since the power that emerges from the slot propagates radially as a TM_0 cylindrical in-phase wavefront. However, a significant part of the power is radiated almost isotropically to free–space giving rise to high side lobes due to the interference of the slot radiation with the in–phase contributions arising from the leaky wave mode sustained by the grating. A solution to minimize them is to use a monopole instead of a slot, since it presents low radiation close to and (ideally null) at broadside and most of the power is directed in the transverse direction.

U. Beaskoetxea, A. E. Torres-García and M. Beruete are with the Antennas Group-TERALAB, Universidad Pública de Navarra (UPNA), Pamplona, 31006, Spain (e-mail: unai.beaskoetxea@unavarra.es; aliciaelena.torres@unavarra.es; miguel.beruete@unavarra.es). M. Beruete is also with the Institute of Smart Cities, Public University of Navarra. This work was supported by the Spanish Ministerio de Economía y Competitividad (MINECO) with contract TEC2014-51902-C2-2-R. U.B and A.T. acknowledge the funding provided by UPNA via the FPI PhD grant program.

In one of the first papers dealing with planar BE antennas [15], it was confirmed that the monopole source led to a reduced radiation at broadside and two opposite main beams at ±41º for a certain frequency/period combination. Nevertheless, with a monopole as primary source, an asymmetric grating is needed to radiate at broadside, as it will be demonstrated below. Here, we present a detailed study of a light, inexpensive and simple to manufacture BE LWA fed by a monopole surrounded by 5 semicircular metallic strips placed asymmetrically on each half of a grounded dielectric disc with high gain broadside radiation. Although in previous works monopoles have been combined with metasurfaces to achieve off-axis beaming with some arbitrary polarization [14], [16], [17], broadside beaming by means of an asymmetric strips grating has not been used before. In addition, such simple strips are comparatively simpler than previously cited structures. The design and numerical results of the antenna are presented, as well as the fabricated prototype along with the experimental results. Due to the fabrication tolerances, a new design incorporating the measured parameters of the manufactured structure was also analyzed and its performance compared with the experimental results.

II. Design Guidelines

For this first analysis, we simulated a grounded dielectric disc (Rogers RT5880, $\varepsilon_r = 2.2$) with height $h = 0.762$ mm and diameter $D = 228$ mm coated with a copper ($\sigma = 5.8\times10^7$ S/m) ground plane of thickness $t = 0.035$ mm. A central monopole (of height $l = \lambda_0/4 = 6$ mm, with $\lambda_0 = 24$ mm the free-space wavelength at the design frequency, $f = 12.5$ GHz) emits a cylindrical wavefront with a phase difference of 180º between upper and lower halves, taking the *x*-*z* plane as the middle plane, as shown in Fig. 1(a), where the phase of the E_y field component at the air-dielectric interface is depicted. So, to get in-phase radiation, it is necessary to implement an asymmetrical BE with a phase difference of 180º between both halves. With this configuration, the antenna is linearly polarized in the *y* direction, as the E_x field component presents opposite phase values at both sides of the *y*-*z* plane due to the vertical symmetry of the periodic structure, see Fig. 1(b), and hence it is canceled, remaining only the E_y component. The grating modulates the surface impedance, giving rise to an infinite number of Floquet harmonics [18]. The angle of radiation θ_n of the *n-th* Floquet mode can be calculated from [5] as $\sin(\theta_n) = (\beta - 2\pi n/d)/k_0$, with β the effective phase constant of the zero order Floquet mode, d the grating period and k_0 the free-space wavenumber. The choice of both β and d is explained below.

This article has been accepted for publication in a future issue of this journal, but has not been fully edited. Content may change prior to final publication. Citation information: DOI 10.1109/LAWP.2018.2791660, IEEE Antennas and Wireless Propagation Letters

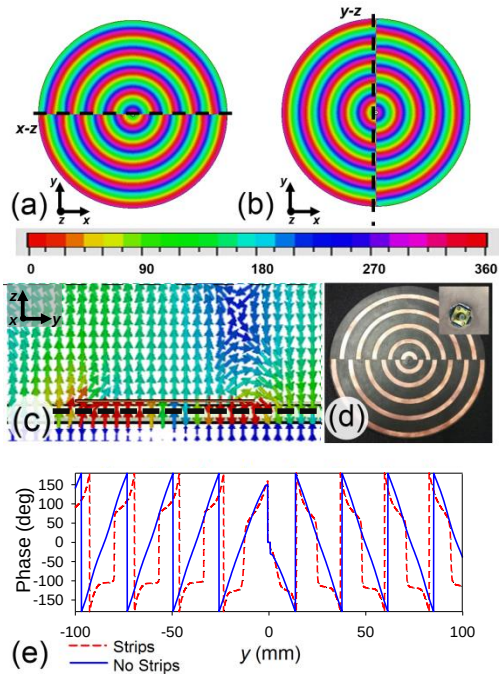

Fig. 1. Phase of the (a) E_y and (b) E_x field components for the unpatterned disc. (c) Cross-section detail of the E-field distribution at the interface for the slab with strips. (d) Photograph of the fabricated antenna (Inset: detail of the SMA). (e) Phase of the H_x field 0.4 mm inside the dielectric slab [represented with a dashed black line in (c)] along the y direction for the patterned (solid blue line) and unpatterned (dashed red line) disc.

The numerically calculated phase constant of the fundamental grounded dielectric slab (transverse magnetic, TM_0) mode is $\beta_0 = 1.006k_0$ at the operation frequency from which we can obtain the attenuation constant in the transversal direction $h/k_0 = 0.109$. Hence, the $1/e$ field decay distance in the air is $1.59\lambda_0$, which means that the mode is loosely confined to the interface. In contrast to [15], the perturbation introduced by the strips is not negligible and we need to consider the excitation of the fundamental quasi-transverse electromagnetic (QTEM) mode of the microstrip waveguide (formed by the strip, dielectric slab and ground plane) which has a phase velocity slower than that of the TM_0 mode at the operation frequency. This, added to the fact that the strip is resonant, results in an effective wavelength shorter than the case without strips where only the TM_0 existed. This is corroborated in Fig. 1(e) by comparing the phase of the H_x field inside the dielectric for the non-patterned (solid blue line) and patterned (dashed red line) cases. As observed, the wavelength for the latter case is shorter, but not too different. So, we can safely assume that the effective propagation constant is $\beta \cong k_0$ and from here we find that with $d \cong \lambda_0 = 24$ mm, a single broadside beam corresponding to the $n = -1$ mode is ensured [5], corresponding the 180° phase difference between both gratings to a difference of $d/2 = \lambda_0/2$.

The distance from the center of the disc to the first strip (offset), critical for a good antenna performance, was obtained by analyzing H_x on the ground plane for the non-patterned case, similarly to previous works [10], [11]. Thus, the upper grating starts at an offset distance o_1, while the lower set starts at $o_2 \cong o_1 + d/2$. Finally, to obtain half-wavelength resonant strips, they were designed following the rules of classical patch antennas with a width w = 7.57 mm [19]. The 180º phase change corresponding to the half-wavelength resonance is observed in Fig. 1(c).

III. Numerical Results

We performed a numerical analysis using the commercial simulator CST Microwave Studio® to obtain the radiation characteristics in the frequency range from f = 11.5 to 15 GHz and for an angular range from –90º to 90º. A relatively low number of periods (5) was used because it is a good trade-off between size and gain and at the same time prevents from having an extremely narrow operation bandwidth. To get a fine-tuned design d, w, o_1, o_2 and l underwent an optimization routine, setting as optimization goals the highest possible gain, minimizing at the same time the side lobe level and the reflection coefficient magnitude at the design frequency.

The analytical values taken as seeds for the optimization, obtained in Section II are summarized in Table I, alongside the optimized values for the ideal design.

TABLE I
Analytical, Ideal And Fabricated Antenna Dimensions

Parameter	Analytical (mm)	Ideal (mm)	Fabricated (mm)
Period, d	24	23.1	22.1 (average)
Strip width, w	7.57	6.6	6.5 (average)
Offset 1, o_1	5	5.7	5.7
Offset 2, o_2	14.5	15.2	14.46
Monopole height, l	6	4.42	4.238

Strip period and width are arguably the most critical parameters to get high gain at broadside. Figure 2 displays the normalized broadside directivity at the operation frequency f = 12.6 GHz for the optimized antenna as a function of d and w. Note that this is the frequency at which the best trade-off between gain and low side lobes is observed, while f = 12.5 GHz was the initial frequency of design. From now on, we will refer to 12.6 GHz as the operation frequency. It is shown that the maximum has strong dependence on w. For example, for a 10% of variation around the central width value (w = 6.6 mm), the gain drops almost 4 dB, whereas for the same percentage variation of the period around d = 23.1 mm, it barely decreases 0.6 dB.

The numerical results of the ideal structure are displayed with green curves in Fig. 3 and are summarized in Table II. The reflection coefficient, inset in Fig. 3(a), presents a dip near the operation frequency, with a minimum at 12.4 GHz. The normalized co-polar radiation diagrams at f = 12.6 GHz for the E- and H-planes are respectively displayed in Fig. 3(b) and (c), whereas the cross-polar planes are shown in Fig. 3(d) and (e). The antenna presents a side lobe level in the E-Plane of about –20.3 dB while, as a comparison, a 5 period version of the design in [10] presents a side lobe level of –12 dB (not shown). Furthermore, the numerical cross-polar component for the E-plane is null due to the imposed magnetic symmetry.

The performance of the LWA was evaluated considering

This article has been accepted for publication in a future issue of this journal, but has not been fully edited. Content may change prior to final publication. Citation information: DOI 10.1109/LAWP.2018.2791660, IEEE Antennas and Wireless Propagation Letters

the attenuation (α_n) and phase constant (β_n) of the radiating mode ($n = -1$ in our case), obtained respectively by means of the Generalized-Pencil-of-Function method [20] and by the equation $\sin(\theta_n) = \beta_n/k_0$ [18]. Thus, the antenna at f = 12.6 GHz has α_{-1} = 0.0154 Np/m and $\beta_{-1} \approx 0$ m^{-1} (corresponding $\beta_{-1} = 0$ to the open stopband [5]). We cross-checked the value of α by means of the equation $\theta_{-3dB} = (2\alpha/k_0)\cos(\theta)$ for which an analytical beamwidth value of θ_{-3dB} = 6.7° was obtained, showing an excellent agreement with the numerical value (6.6°), and a 97% of radiated power. However, the calculated aperture efficiency (11.49%) shows that the surface illumination is poor. To optimize it, a non-purely exponentially decreasing attenuation should be implemented [14], but this is beyond the scope of this work.

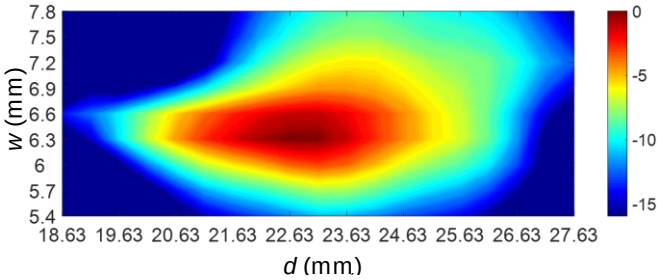

Fig. 2. Normalized directivity (dB) at broadside as a function of the width of the strips (w) and the period of the grating (d) for f = 12.6 GHz.

TABLE II
NUMERICAL AND EXPERIMENTAL RESULTS

	Ideal @12.6 GHz	Measured @13 GHz	Adjusted @12.75 GHz
Gain (dBi)	20.17	19.4	19.3
Aperture Efficiency, e_a	11.49 %	9.45 %	9.24 %
θ_{-3dB}*	6.6º	6º	6.2º
θ_{-3dB}**	9.4º	9º	8.6º
Side Lobe Level (dB)*	–20.3	–16	–17.7
Side Lobe Level (dB)**	–37.6	–28	–20.8

* and ** refer to E– and H–plane, respectively.

IV. FABRICATED STRUCTURE AND EXPERIMENTAL RESULTS

The manufactured antenna [Fig. 1(d), with inset showing the welded SMA coaxial connector], was patterned by means of a computer numeric control milling machine and has a weight of 78.6 g. The core was cut above the optimized value and then progressively trimmed until the resonance was obtained at the desired frequency. This was done due to the non-ideality of the material employed for the fabrication, the inaccuracies of the patterning and the sensitivity of the reflection coefficient to the monopole length. A further inspection of the prototype revealed small errors in the fabrication process. The values for d, w, o_1, o_2 and l are included in Table I. The experimental reflection coefficient, recorded from 11.5 to 15 GHz, is displayed with a dashed blue line in the inset of Fig. 3(a). A frequency shifting of the dip towards 12.65 GHz as well as an increase of the Q-factor is noticed. This frequency shift can be related to the variation of the observed impedance at the output of the SMA produced by the deviation of the offset distance in the x direction.

For the experimental broadband gain and the radiation diagrams characterization, the gain-comparison method was applied. The broadband gain was obtained from 11.5 to 15 GHz and the farfield diagrams from –80º to 80º at 12.6 GHz and the results are displayed with dashed blue lines in Fig. 3. The deviation of the monopole with respect to the center of the disc results in an out-of-phase interaction of the scattered waves producing a ~450 MHz blueshift and decrease of the broadband gain compared with the ideal case (~2.4 dB decrease), angle tilting of the maximum gain beam (2º heeled from broadside in both E- and H-planes) and higher side lobe levels (6.55 dB higher). As the symmetry of the structure is broken due to the shift of the monopole from the center of the structure, a non-null cross-polar value for the E-plane is observed, remaining anyway lower than –35 dBi at broadside. However, at f = 13 GHz, it is observed a gain of 19.4 dBi along with a –16 dB side lobe level and a 6º beamwidth, in good agreement with the observed blueshift of the response. These values at 13 GHz are summarized in Table II.

With the intention of being more rigorous (i.e, checking the effect of the fabrication deviations), we simulated a new design (labelled as "adjusted") that incorporated the dimensions of the fabricated structure. Despite measuring every single dimension of the prototype, we were not able to accurately replicate it, as it can be seen in the results, plotted with red dotted lines in Fig. 3. Again, at higher frequencies (f = 12.75 GHz), a better behavior is observed with a gain of 19.3 dBi and –17.7 dB side lobe level. The numerical results at 12.75 GHz are summarized in Table II.

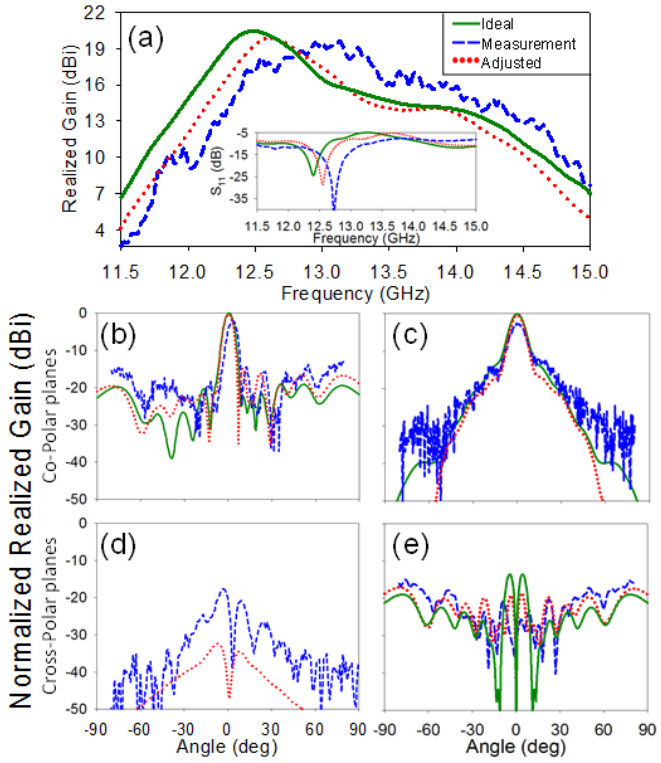

Fig. 3. Simulation results for ideal (green solid lines) and adjusted (red dotted lines) antenna along with the experimental results (blue dashed lines) of the manufactured prototype. (a) Broadband realized gain (Inset: reflection coefficient magnitude). Normalized diagrams at 12.6 GHz for co-polar (b) E-plane and (c) H-plane and cross-polar (d) E-plane and (e) H-plane.

This article has been accepted for publication in a future issue of this journal, but has not been fully edited. Content may change prior to final publication. Citation information: DOI 10.1109/LAWP.2018.2791660, IEEE Antennas and Wireless Propagation Letters

The realized gain as a function of angle and frequency for both measured and adjusted E- and H-planes is mapped in Fig. 4. A gain exceeding 10 dBi is observed at broadside from 12 to 14.5 GHz, and near the operating frequency it peaks more than 18 dBi. The analytical beam directions are overlapped in Fig. 4(a), with a clear trend of the mode $n = -1$ (curves around $\theta = 0^{\circ}$), while mode $n = -2$, due to the lower gain displayed, is less noticeable.

The inaccuracies in the replication of the results could also correspond to reasons other than the design itself: variation of the ε_r, bending of the disc during the patterning, tilting of the monopole or even experimental inaccuracies, such as setup misalignments. Despite all these issues, measurement and simulation results show overall good agreement for both ideal and adjusted antennas and prove the feasibility of a broadside beaming antenna using a monopole and an asymmetric pattern and that, once mastered the manufacturing process, interesting and competitive prototypes can be obtained.

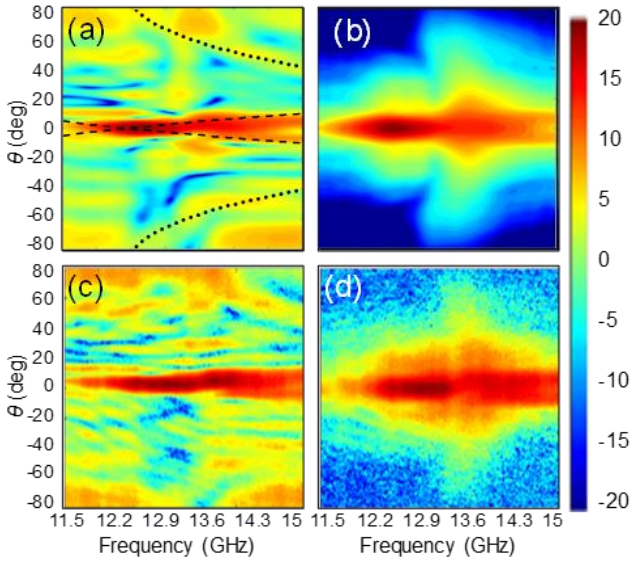

Fig. 4. Realized gain as a function of angle and frequency: adjusted simulated (a) E-plane and (b) H-plane, and measured (c) E-plane and (d) H-plane.

V. Conclusions

A grounded dielectric slab based BE LWA fed by a central monopole surrounded by asymmetric semicircular strips has been presented. The experimental results show a frequency shift of the response of the antenna with respect to the ideal simulated case due mainly to the fabrication tolerances, displaying at $f = 13$ GHz a high gain of 19.4 dBi (ideally 20.17 dBi) and side lobe level of –16 dB (–20.3 dB for the ideal simulated case) alongside a beamwidth $\theta_{-3dB} = 6^{\circ}$. The use of a monopole as feeding source instead of a radiating resonant slot was proposed to reduce side lobe levels, as it presents a null in transmission in broadside and maximum at endfire directions, unlike the slot, which presents high direct-to-free-space transmission and, hence, higher side lobe levels. In addition, this structure has the added value of its lightweight, easy and cost-effective fabrication. This antenna might be of interest for space applications in Ku band where lightweight and reduced volumes are required.

Acknowledgement

The authors are grateful to Dr. Enrica Martini for her GPOF-method-code and to Prof. Stefano Maci for the initial idea of the asymmetric Bull's-Eye antenna and his valuable comments regarding its physical operation.

References

[1] L. Martín-Moreno *et al.*, "Theory of Extraordinary Optical Transmission through Subwavelength Hole Arrays," *Phys. Rev. Lett.*, vol. 86, no. 6, pp. 1114–1117, Feb. 2001.

[2] H. J. Lezec *et al.*, "Beaming Light from a Subwavelength Aperture," *Science*, vol. 297, no. 5582, pp. 820–822, Aug. 2002.

[3] M. Beruete *et al.*, "Enhanced millimeter-wave transmission through subwavelength hole arrays," *Opt. Lett.*, vol. 29, no. 21, p. 2500, Nov. 2004.

[4] M. Beruete *et al.*, "Enhanced microwave transmission and beaming using a subwavelength slot in corrugated plate," *IEEE Antennas Wirel. Propag. Lett.*, vol. 3, no. 1, pp. 328–331, Dec. 2004.

[5] D. R. Jackson *et al.*, "Beaming of light at broadside through a subwavelength hole: Leaky wave model and open stopband effect," *Radio Sci.*, vol. 40, no. 6, Dec. 2005.

[6] F. Monticone and A. Alù, "Leaky-Wave Theory, Techniques, and Applications: From Microwaves to Visible Frequencies," *Proc. IEEE*, vol. 103, no. 5, pp. 793–821, 2015.

[7] M. Beruete *et al.*, "Very Low Profile and Dielectric Loaded Feeder Antenna," *IEEE Antennas Wirel. Propag. Lett.*, vol. 6, no. 99, pp. 544–548, 2007.

[8] M. Beruete *et al.*, "Low-Profile Corrugated Feeder Antenna," *IEEE Antennas Wirel. Propag. Lett.*, vol. 4, no. 1, pp. 378–380, 2005.

[9] M. Beruete *et al.*, "Very Low-Profile 'Bull' s-Eye' Feeder Antennao," *IEEE Antennas Wirel. Propag. Lett.*, vol. 4, pp. 365–368, 2005.

[10] U. Beaskoetxea *et al.*, "77-GHz High-Gain Bull's-Eye Antenna With Sinusoidal Profile," *IEEE Antennas Wirel. Propag. Lett.*, vol. 14, pp. 205–208, 2015.

[11] U. Beaskoetxea *et al.*, "3-D-Printed 96 GHz Bull's-Eye Antenna With Off-Axis Beaming," *IEEE Trans. Antennas Propag.*, vol. 65, no. 1, pp. 17–25, Jan. 2017.

[12] U. Beaskoetxea and M. Beruete, "High Aperture Efficiency Wide Corrugations Bull's-Eye Antenna Working at 60 GHz," *IEEE Trans. Antennas Propag.*, vol. 65, no. 6, pp. 3226–3230, Jun. 2017.

[13] M. D'Auria *et al.*, "3-D Printed Metal-Pipe Rectangular Waveguides," *IEEE Trans. Components, Packag. Manuf. Technol.*, vol. 5, no. 9, pp. 1339–1349, Sep. 2015.

[14] G. Minatti *et al.*, "Synthesis of Modulated-Metasurface Antennas With Amplitude, Phase, and Polarization Control," *IEEE Trans. Antennas Propag.*, vol. 64, no. 9, pp. 3907–3919, Sep. 2016.

[15] P. Baccarelli *et al.*, "A novel printed leaky-wave 'bull-eye' antenna with suppressed surface-wave excitation," in *IEEE Antennas and Propagation Society Symposium, 2004.*, vol. 1, pp. 1078–1081.

[16] S. Pandi *et al.*, "Design of Scalar Impedance Holographic Metasurfaces for Antenna Beam Formation With Desired Polarization," *IEEE Trans. Antennas Propag.*, vol. 63, no. 7, pp. 3016–3024, Jul. 2015.

[17] M. Casaletti *et al.*, "Polarized Beams Using Scalar Metasurfaces," *IEEE Trans. Antennas Propag.*, vol. 64, no. 8, pp. 3391–3400, Aug. 2016.

[18] A. A. Oliner, "Radiating periodic structures: analysis in terms of k vs. β diagrams," *Short Course Microw. F. Netw. Tech.*, 1963.

[19] I. J. Bahl and P. Bhartia, *Microstrip Antennas*. Artech House, Incorporated, 1980.

[20] Y. Hua and T. K. Sarkar, "Generalized pencil-of-function method for extracting poles of an EM system from its transient response," *IEEE Trans. Antennas Propag.*, vol. 37, no. 2, pp. 229–234, Feb. 1989.